Prediction of Disease-Related Femur Shape Changes Using Geometric Encoding and Clinical Context on a Hip Disease CT Database

Ganping Li[1], Yoshito Otake[1], Mazen Soufi[1], Masachika Masuda[1], Keisuke Uemura[2], Masaki Takao[3], Nobuhiko Sugano[4], and Yoshinobu Sato[1]

[1] Division of Information Science, Graduate School of Science and Technology, Nara Institute of Science and Technology, Japan
{li.ganping.lc2,otake,yoshi}@is.naist.jp
[2] Department of Orthopaedics, Osaka University Graduate School of Medicine, Japan
[3] Department of Bone and Joint Surgery, Ehime University Graduate School of Medicine, Japan
[4] Department of Orthopaedic Medical Engineering, Osaka University Graduate School of Medicine, Japan

Abstract. The accurate prediction of femur shape changes due to hip diseases is potentially useful for early diagnosis, treatment planning, and the assessment of disease progression. This study proposes a novel pipeline that leverages geometry encoding and context-awareness mechanisms to predict disease-related femur shape changes. Our method exploits the inherent geometric properties of femurs in CT scans to model and predict alterations in bone structure associated with various hip diseases, such as osteoarthritis (OA). We constructed a database of 367 CT scans from patients with hip OA, annotated using a previously developed bone segmentation model and an automated OA grading system. By combining geometry encoding and clinical context, our model achieves femur surface deformation prediction through implicit geometric and clinical insights, allowing for the detailed modeling of bone geometry variations due to disease progression. Our model demonstrated moderate accuracy in a cross-validation study, with a point-to-face distance (P2F) of 1.545mm on the femoral head, aligning with other advanced predictive methods. This work marks a significant step toward personalized hip disease treatment, offering a valuable tool for clinicians and researchers and aiming to enhance patient care outcomes.

Keywords: Bones · Shape Prediction · Point Cloud Deep Networks · Geometry Encoding · Clinical Context.

1 Introduction

Hip osteoarthritis (OA) poses significant public health challenges, linking to chronic pain, functional disability, and hip replacement surgeries [5]. The disease progression alters femur shape, making accurate prediction critical for diagnosing hip diseases and for the medical research into OA trajectories [23].

However, this task is challenging due to the subtle initial differences between normal and diseased femurs, which become more pronounced and varied as the disease progresses.

Recent progress in deep learning (DL) for predicting anatomical shape deformations requires large longitudinal datasets, whose acquisition is time-consuming and laborious. For instance, Calivá et al. [3] gathered a large-scale longitudinal dataset of MRI images from 2394 patients, taken annually over two years, to study changes in the distal femur. A similar data requirement was also present in cranial implant prediction [27]. In contrast, statistical shape models (SSMs) offer a way to use smaller datasets by focusing on the major variations within the data [20]. However, the inherent linearity of conventional SSMs limits their effectiveness and breadth of application [2,7,8,12]. To address this limitation, recent works like FlowSSM [14] and Mesh2SSM [12] have introduced non-linear elements into SSM, enhancing accuracy and flexibility. FlowSSM, for instance, enables landmark-free modeling through a neural flow deformer, while Mesh2SSM uses sparse correspondences and unsupervised learning for better shape analysis. Despite these advancements, such methods ignore the potential of integrating clinical context into spatial data, which could yield additional insights into patient-specific conditions. Our approach bridges this gap by integrating geometric shape analysis with clinical context awareness [17,11,25,29], aiming to uncover latent correlations between surface deformations and clinical conditions. The strategy employs demographic and pathological data, which are known to influence femoral morphology [26], as auxiliary information alongside geometric details, offering a more comprehensive analysis than traditional methods.

This study develops a comprehensive pipeline to predict femur shape changes resulting from hip OA progression, using partially diseased CT scans and demographic data. Given the challenges in acquiring longitudinal datasets, the model predicts the femur shape of the diseased lateral using the contralateral, normal lateral from the same patient's CT scan. This approach is based on the proven symmetry between bilateral femurs, as documented in [30]. Our approach overcomes the limitations of previous SSM-based and DL-based methods by integrating geometric encoding and clinical context awareness mechanisms. Conceptually, a segmentation model and an OA grading model are deployed to extract bone labels and pathological data from CT scans. Subsequently, a multilayer perceptron (MLP)-based model is trained to fuse geometric features and clinical context for femur shape prediction. This tool could assist researchers in precisely delineating patient trajectories and facilitate the exploration of intervention effects, such as hip joint implants, on predicted bone remodeling.

The contribution of this paper is threefold: 1) a comprehensive pipeline is proposed for predicting femur shape changes from the normal bone shape of the same patient. This enhances prediction accuracy with limited data by incorporating geometric encoding and clinical context; 2) the impact of incorporating geometric encoding and clinical context on the accuracy of shape prediction is validated; 3) the effectiveness of the proposed pipeline is demonstrated using a

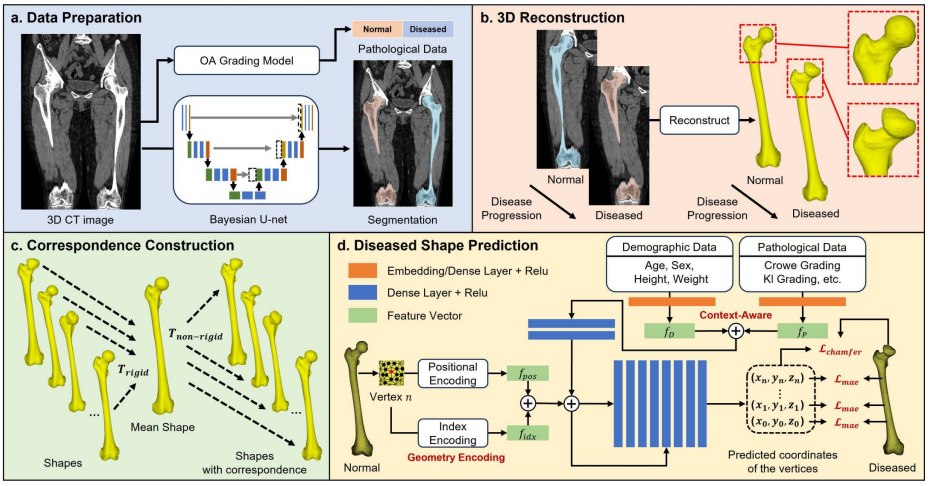

Fig. 1. Overview of the Proposed Pipeline: **a. Data Preparation** employs a pre-trained Bayesian U-net and a hip OA grading model for CT scan segmentation and OA grading. Then, classifies segmented images into normal or diseased based on pathology labels. **b. 3D Reconstruction** mesh reconstruction and refinement. **c. Correspondence Construction** uses group-wise registration to create a mean shape for the non-rigid fitting of all surfaces. **d. Diseased Shape Prediction** vertex-wisely predicts the diseased femur shape from the patient's normal surface and clinical data.

non-longitudinal dataset of 367 lower extremity CT scans from patients with unilateral hip joint osteoarthritis (OA), as a proof-of-concept experiment.

2 Method

The overview of the proposed pipeline is illustrated in Figure 1. This section provides detailed explanations of the data preparation process and descriptions of each module involved in predicting diseased femur shapes from normal laterals.

2.1 Dataset Preparation

We collected a dataset of CT images comprising 367 preoperative scans of the lower extremities from patients aged 17 to 87, all diagnosed with unilateral hip joint osteoarthritis. This dataset also includes demographic information such as sex, age, height, and weight. Each CT image was trimmed to the region of interest (ROI) from the iliac crest to the knee joint beforehand, and the shape is (512, 512, n) with element spacing of $(0.7, 0.7, 1.0)$, where $n \in [526, 700]$.

Figure 1.a and Figure 2 illustrate the bone and pathological data extraction process for our study. Initially, femur labels were extracted from CT images using a pre-trained 5-layer Bayesian U-net [9], as depicted in Figure 1.a. Simultaneously, each CT image was projected onto the anteroposterior plane (AP) to

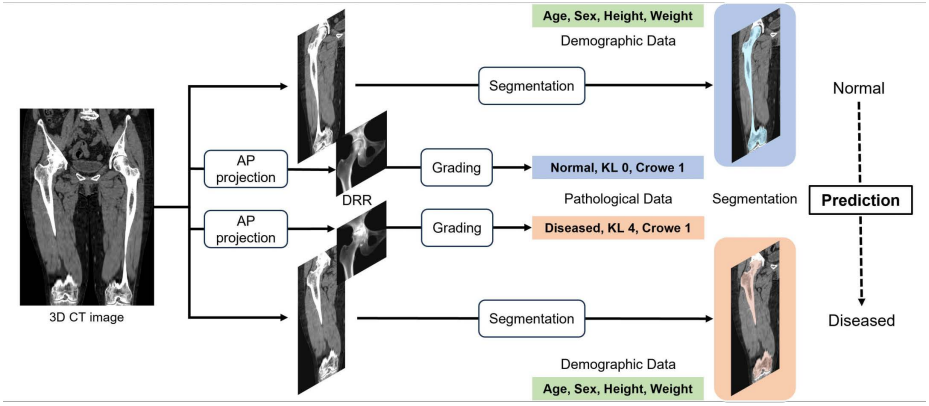

Fig. 2. Diagram of bone shape and pathological data preparation.

create a digitally reconstructed radiograph (DRR) of the hip joint's ROI. From this DRR, a pre-trained ViT-based model [15] automatically assigned Crowe and Kellgren and Lawrence (KL) grades [13] for OA assessment. The dataset features Crowe grades ranging from 0 to 3 and KL grades from 0 to 4. After associating the segmentation label with OA grades, the CT image was bifurcated into two parts: the healthier (normal) lateral of lower Crowe and KL grades, and the diseased lateral of higher grades. The accuracy (mean $\pm$ std) of the segmentation model is DC: 0.991 $\pm$ 0.005 and ASD: 0.152 $\pm$ 0.384 mm. The accuracy of the OA grading model is 0.955 $\pm$ 0.021 for one-neighbor and 0.649 $\pm$ 0.023 for exact class, with the predictions verified by medical experts.

As depicted in Figure 1.b, both normal and diseased laterals were converted and remeshed into 3D meshes of 8192 vertices using the Visualization Toolkit (VTK) [19] and Approximated Centroidal Voronoi Diagrams (ACVD) [22], to balance surface details and computational cost. Then in Figure 1.c, we performed a group-wise registration of all surfaces with reference identification via ShapeWorks [4]. To establish surface correspondences, we non-rigidly adjusted the mean shape to fit the other surfaces using a geodesic-based Bayesian Coherent Point Drift (BCPD) method [10]. The distance error for registration is 1.104 $\pm$ 0.131 mm (mean $\pm$ std). Finally, all surfaces were aligned to the reference in preparation for subsequent experiments.

2.2 Shape Prediction

Geometry Encoding and Clinical Context To effectively utilize spatial information from vertex coordinates and correspondence, we involve a method called geometry encoding to convert coordinates to high-dimensional features. This approach allows precisely encoding each vertex on surfaces by positional and index encoding. Unlike its usage in transformers, positional encoding transforms vertex coordinates into a higher-dimensional space using high-frequency

sinusoidal functions, enhancing the network's ability to detect subtle variations [16]. Index encoding, conversely, assigns unique indices to each vertex to maintain structural integrity and positional relationships, thus aiding the network in learning complex geometric details.

Furthermore, we propose a clinical context module that fuses demographic (age, sex, height, weight) and pathological data, including Crowe and KL grades for the normal lateral, as well as the OA grade difference between both laterals. Empirically, embedding only the OA grade of either the normal or diseased lateral leads to generating homogeneous shapes. This is implemented by embedding categorical data (e.g., sex) or processing continuous data (e.g., age) through a fully connected layer, resulting in two vectors. These vectors are then merged and processed through a 2-layer dense network to serve as a comprehensive clinical feature, offering contextual insights for enhanced model performance.

Proposed Backbone An MLP-based model $F_\theta : (x, C) \rightarrow y$ is designed to fuse geometry and, optionally, clinical information for shape prediction, as illustrated in Figure 1.d. During the training phase, 3-D coordinate of vertex x_{ij} on a normal surface S_j is encoded to a 63-D position feature vector f_{pos} and a 32-D index feature vector f_{idx} by geometry encoding. The two vectors are then concatenated to form the geometric feature of x_{ij}. Concurrently, clinical data C_j associated with S_j is embedded into a 128-D clinical feature vector, derived from multiple 32-D demography features f_D and pathology features f_P, using a 2-layer dense network. Subsequently, these two types of feature vectors are fused and input into an MLP network, adapted from the decoder in [6]. The weights θ are optimized by mean absolute error (MAE) between the predicted vertex $\hat{y}_{ij}$ and those y_{ij} of the ground truth (GT) diseased shape V_j, as well as the L1 Chamfer Distance (CD) between the predicted vertex locations $\hat{V}_j$ and V_j. The loss function is described as follows:

$$\mathcal{L}_{\text{total}} = \frac{1}{M} \sum_{j=1}^{M} \left(\frac{1}{N_j} \sum_{i=1}^{N_j} |\hat{y}_{ij} - y_{ij}| + \lambda \cdot \mathcal{L}_{\text{1Chamfer}}(\hat{V}_j, V_j) \right) \tag{1}$$

where λ, M, and N are the weight, number of training shapes, and number of vertices in the surface, respectively. λ is set to 10 in all experiments. This integrated approach enables the model to make more informed decisions, effectively enhancing its ability to discern subtle distinctions and patterns within the deformation that geometric features alone may not fully capture.

Point Cloud Models To assess the validity of our proposed model, we perform comparative experiments using the autoencoder (AE) variants of several state-of-the-art point cloud networks (PCNs) as the foundation for shape prediction. These models include: **PointNet[18]** (convolution-based), **DGCNN[24]** (Dynamic Graph CNN, convolution-based with edge convolution), and **SFN[28]** (SnowflakeNet, transformer-based). For a fair comparison, we adhere to the default hyperparameter settings provided that achieve the best performance among

the officially provided templates and conduct training trials three times using L1 CD loss, MAE loss, or $\mathcal{L}_{\text{total}}$. The best-performing results by each loss type are selected for comparison. Non-linear SSMs are not compared here as their strength lies in descriptively capturing subtle variances. However, future work will include their evaluation, focusing on a flexible representation of shapes for predictive tasks.

2.3 Evaluation Metrics

To thoroughly evaluate our model, we utilize several metrics: the F-score [21], point-to-face (P2F) distance, Hausdorff distance (HD), HD95, the Earth Mover's Distance (EMD), and the L1 and L2 Chamfer Distance (CD). The F-score measures reconstruction accuracy by calculating the percentage of correctly predicted points, providing insight into the model's overall performance. On the other hand, the P2F distance assesses surface sampling precision by computing the average distance from each predicted point to the nearest surface on the ground truth mesh [1]. The P2F, CD, and HD focus on measuring geometric discrepancies and spatial accuracy between shapes, while the EMD and the F-score evaluate the overall similarity and completeness of the model predictions.

3 Experiments and Results

We conducted experiments across all PCN models and two proposed methods: 1) **GE** (MLP with geometry encoding) to validate our proposed backbone's effectiveness; and 2) **GE+CCA** (GE enhanced with clinical context awareness), to assess the impact of the context-awareness module, also serving as an ablation study. Our experiments use the Normal-Diseased baseline, which considers the GT difference between normal and diseased laterals, reflecting the variation in femur deformation at different OA progression stages. We employed a 10-fold cross-validation across all methods on our femur shape dataset. During training, we reserve 10% of the surfaces as a validation set for each fold. For PCN models, our combined loss, $\mathcal{L}_{\text{total}}$, yielded the best results on DGCNN, whereas CD loss was most effective on PointNet and SFN. Note that all PCNs use only geometry information for training. Considering the proximal femur's sensitivity to OA progression, our evaluation focus was on the upper quarter of the femur.

Observations on the dataset indicate that femur shape variations are more constrained among patients with minor OA grade differences between hip joints. Therefore, to enhance clinical utility, our study specifically targets patients with a lateral KL grade discrepancy of 4 and a Crowe grade discrepancy greater than 0. The average performance across seven metrics is presented in Table 1, and we put the full results in the supplementary material. One can infer that GE surpasses the baseline and all PCNs in every metric with limited training data (around 300 cases). This highlights the effectiveness of the proposed MLP + geometry encoding model in leveraging correspondence and spatial data across normal and diseased laterals. The method achieves a high F-score close

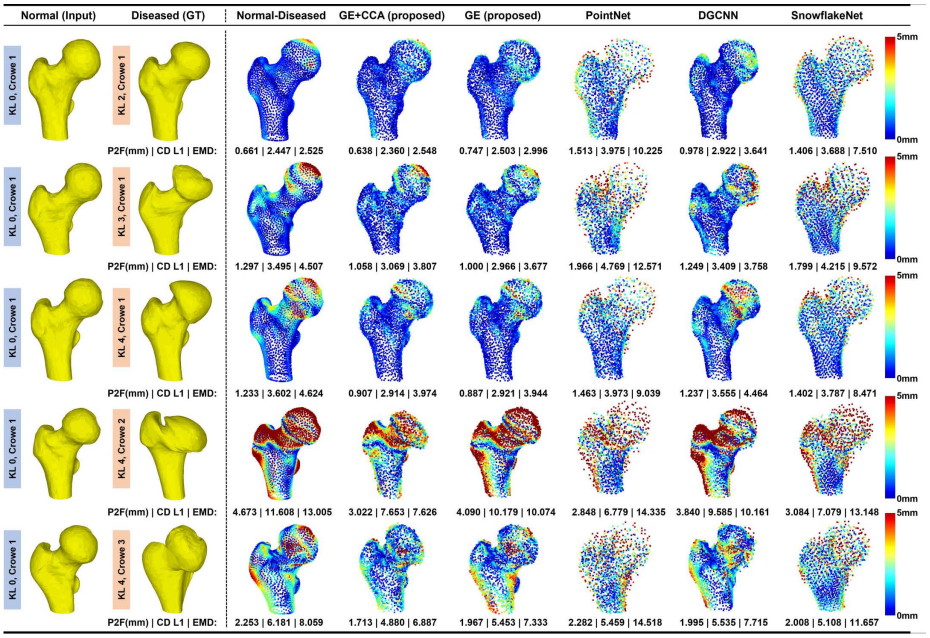

Fig. 3. Comparative shape prediction results for different disease progression degrees. P2F and EMD results are attached to show spatial accuracy and distribution similarity between prediction and ground truth (GT). From left to right, it includes input surfaces (normal), GT of the diseased lateral, the deviation between GT of normal and diseased laterals, and predictions from all methods. Vertically, the display features representative cases of five distinct stages of hip joint disease progression on the diseased lateral: KL 2, Crowe 1, KL 3, Crowe 1, KL 4, Crowe 1, KL 4, Crowe 2, and KL 4, Crowe 3.

to the baseline, indicating reasonable shape completeness in our shape predictions. When integrated with CCA, our model shows modest improvements over the baseline by fusing supplemental demographic and pathological data, evidenced by a decrease in P2F by around 0.09, L_1 CD by 0.36, and HD by about 1.2. Among the PCNs, spatial accuracy measures results were unsatisfactory. However, DGCNN scores relatively well in F-score and EMD, benefiting from correspondence and the geometric relationships captured by k-nearest neighbors (KNN). SFN, despite being proven effective in learning point cloud representations using small-scale datasets [1], demonstrated a less impressive performance in capturing deformations from normal to diseased states.

In each progression stage, we select typical cases and envision their pathological accuracy through the P2F distance to the ground truth, as visualized in Figure 3. This illustrates that our GE + CCA method effectively preserves geometric features, even in mildly ill cases where the deviation from the normal lateral is minimal (see the 1st row). In scenarios involving severe deformations of the femoral head and neck, as shown in the 4th row, our method still manages to

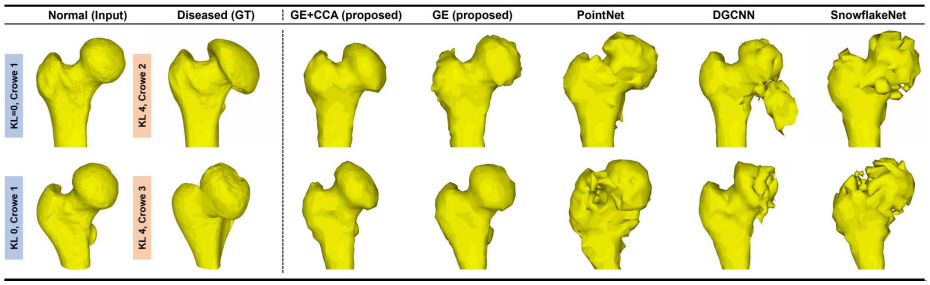

Fig. 4. Visualization of surface reconstruction across various methods for two representative samples, where GE and GE + CCA are our proposed methods.

Table 1. Comparative analysis of average evaluation metrics for point predictions using various methods, where GE and GE + CCA are our proposed methods. F-score is computed with a 1% threshold relative to the shape's bounding box diagonal. The best prediction values are shown in bold.

Grade Diff.	Method	Metrics						
		P2F(mm)↓	CD L1↓	CD L2↓	HD↓	HD95↓	F-score↑	EMD↓
KL 4 Crowe 0-2 262 Cases	N-D*	1.630	4.618	5.613	11.251	5.639	0.421	5.409
	PointNet	1.864	4.885	5.743	13.368	5.355	0.265	11.817
	DGCNN	1.928	5.015	6.050	12.037	6.043	0.326	5.584
	Snowflake	1.951	4.853	5.660	12.477	5.203	0.260	10.032
	GE	1.583	4.316	5.154	10.443	4.972	0.416	5.179
	GE + CCA	**1.545**	**4.257**	**5.074**	**10.066**	**4.941**	**0.418**	**5.170**

* Direct comparison between the ground truth of normal and diseased laterals.

predict the direction of deformation based on clinical information. Furthermore, we reconstruct the proximal femur from point predictions in two representative cases with high osteoarthritis (OA) grades, offering a qualitative view of the prediction's uniformity.

Limitations and Future Works Two major limitations of our proposed pipeline need to be addressed. Firstly, the performance of our model is affected by the quality of image segmentations and clinical data, which results in modest enhancements over the baseline Table 1. Despite incorporating Bayesian estimation in our upstream models [9,15] to improve validity, our pipeline's two-stage process may still amplify initial errors. Secondly, our model focuses exclusively on surface correspondence and overlooks the local geometric relationships, evident from the rough surfaces observed around areas such as the greater trochanter (see Figure 4). Future efforts will aim to improve pipeline robustness, enhance model reliability in clinical settings through probability calibration, and increase accuracy by incorporating edge feature extraction. Additionally, a longitudinal dataset is being collected for more comprehensive comparisons.

4 Conclusions

This study introduces a novel pipeline* for predicting femur shape changes due to hip OA progression from normal lateral, leveraging geometry encoding and clinical context awareness. This approach overcomes the limitations of previous SSM-based and DL-based models by effectively utilizing surface correspondence for geometric feature extraction. Our MLP-based fusion model integrates patient demographics and hip OA grades, providing superior geometric and clinical insights compared to standard PCN models across multiple metrics. Furthermore, our pipeline's design facilitates the easy incorporation of new clinical data types and holds the potential to predict femur shapes with specific hip OA states. Although further accuracy improvements and validation are necessary for application in real clinical scenarios, our pipeline reveals a potential multi-modality pathway for femur deformation prediction.

Acknowledgments. This work was funded by MEXT/JSPS KAKENHI (19H01176, 20H04550, 21K16655, 21K18080).

Disclosure of Interests. The authors have no competing interests to declare that are relevant to the content of this article.

References

1. Adams, J., Elhabian, S.Y.: Can point cloud networks learn statistical shape models of anatomies? In: International Conference on Medical Image Computing and Computer-Assisted Intervention. pp. 486–496. Springer (2023)
2. Bowes, M.A., Kacena, K., Alabas, O.A., Brett, A.D., Dube, B., Bodick, N., Conaghan, P.G.: Machine-learning, mri bone shape and important clinical outcomes in osteoarthritis: data from the osteoarthritis initiative. Annals of the rheumatic diseases **80**(4), 502–508 (2021)
3. Calivá, F., Kamat, S., Martinez, A.M., Majumdar, S., Pedoia, V.: Surface spherical encoding and contrastive learning for virtual bone shape aging. Medical Image Analysis **77**, 102388 (2022)
4. Cates, J., Elhabian, S., Whitaker, R.: Shapeworks: particle-based shape correspondence and visualization software. In: Statistical shape and deformation analysis, pp. 257–298. Elsevier (2017)
5. Charlesworth, J., Fitzpatrick, J., Perera, N.K.P., Orchard, J.: Osteoarthritis-a systematic review of long-term safety implications for osteoarthritis of the knee. BMC musculoskeletal disorders **20**, 1–12 (2019)
6. De Luigi, L., Cardace, A., Spezialetti, R., Zama Ramirez, P., Salti, S., Di Stefano, L.: Deep learning on implicit neural representations of shapes. In: International Conference on Learning Representations (ICLR) (2023)
7. Goparaju, A., Iyer, K., Bone, A., Hu, N., Henninger, H.B., Anderson, A.E., Durrleman, S., Jacxsens, M., Morris, A., Csecs, I., et al.: Benchmarking off-the-shelf statistical shape modeling tools in clinical applications. Medical Image Analysis **76**, 102271 (2022)

*The source code is available at: https://github.com/RIO98/FemurSurfacePrediction

8. Grassi, L., Väänänen, S.P., Isaksson, H.: Statistical shape and appearance models: Development towards improved osteoporosis care. Current Osteoporosis Reports **19**, 676–687 (2021)
9. Hiasa, Y., Otake, Y., Takao, M., Ogawa, T., Sugano, N., Sato, Y.: Automated muscle segmentation from clinical ct using bayesian u-net for personalized musculoskeletal modeling. IEEE transactions on medical imaging **39**(4), 1030–1040 (2019)
10. Hirose, O.: Geodesic-based bayesian coherent point drift. IEEE Transactions on Pattern Analysis and Machine Intelligence **45**(5), 5816–5832 (2022)
11. Höhn, J., Krieghoff-Henning, E., Jutzi, T.B., von Kalle, C., Utikal, J.S., Meier, F., Gellrich, F.F., Hobelsberger, S., Hauschild, A., Schlager, J.G., et al.: Combining cnn-based histologic whole slide image analysis and patient data to improve skin cancer classification. European journal of cancer **149**, 94–101 (2021)
12. Iyer, K., Elhabian, S.Y.: Mesh2ssm: From surface meshes to statistical shape models of anatomy. In: International Conference on Medical Image Computing and Computer-Assisted Intervention. pp. 615–625. Springer (2023)
13. Kellgren, J.H., Lawrence, J.: Radiological assessment of osteo-arthrosis. Annals of the rheumatic diseases **16**(4), 494 (1957)
14. Lüdke, D., Amiranashvili, T., Ambellan, F., Ezhov, I., Menze, B.H., Zachow, S.: Landmark-free statistical shape modeling via neural flow deformations. In: International Conference on Medical Image Computing and Computer-Assisted Intervention. pp. 453–463. Springer (2022)
15. Masuda, M., Soufi, M., Otake, Y., Uemura, K., Kono, S., Takashima, K., Hamada, H., Gu, Y., Takao, M., Okada, S., et al.: Automatic hip osteoarthritis grading with uncertainty estimation from computed tomography using digitally-reconstructed radiographs. International Journal of Computer Assisted Radiology and Surgery (2024)
16. Mildenhall, B., Srinivasan, P.P., Tancik, M., Barron, J.T., Ramamoorthi, R., Ng, R.: Nerf: Representing scenes as neural radiance fields for view synthesis. Communications of the ACM **65**(1), 99–106 (2021)
17. Pei, L., Vidyaratne, L., Rahman, M.M., Iftekharuddin, K.M.: Context aware deep learning for brain tumor segmentation, subtype classification, and survival prediction using radiology images. Scientific Reports **10**(1), 19726 (2020)
18. Qi, C.R., Su, H., Mo, K., Guibas, L.J.: Pointnet: Deep learning on point sets for 3d classification and segmentation. In: Proceedings of the IEEE conference on computer vision and pattern recognition. pp. 652–660 (2017)
19. Schroeder, W., Martin, K., Lorensen, B.: The Visualization Toolkit (4th ed.). Kitware (2006)
20. Sholukha, V., Chapman, T., Salvia, P., Moiseev, F., Euran, F., Rooze, M., Jan, S.V.S.: Femur shape prediction by multiple regression based on quadric surface fitting. Journal of Biomechanics **44**(4), 712–718 (2011)
21. Tatarchenko, M., Richter, S.R., Ranftl, R., Li, Z., Koltun, V., Brox, T.: What do single-view 3d reconstruction networks learn? In: Proceedings of the IEEE/CVF conference on computer vision and pattern recognition. pp. 3405–3414 (2019)
22. Valette, S., Chassery, J.M.: Approximated centroidal voronoi diagrams for uniform polygonal mesh coarsening. In: Computer Graphics Forum. vol. 23, pp. 381–389. Wiley Online Library (2004)
23. Van Buuren, M., Arden, N.K., Bierma-Zeinstra, S., Bramer, W.M., Casartelli, N.C., Felson, D., Jones, G., Lane, N.E., Lindner, C., Maffiuletti, N.A., et al.: Statistical shape modeling of the hip and the association with hip osteoarthritis: a systematic review. Osteoarthritis and cartilage **29**(5), 607–618 (2021)

24. Wang, Y., Sun, Y., Liu, Z., Sarma, S.E., Bronstein, M.M., Solomon, J.M.: Dynamic graph cnn for learning on point clouds. ACM Transactions on Graphics (tog) **38**(5), 1–12 (2019)
25. Wang, Y., Cai, J., Louie, D.C., Wang, Z.J., Lee, T.K.: Incorporating clinical knowledge with constrained classifier chain into a multimodal deep network for melanoma detection. Computers in Biology and Medicine **137**, 104812 (2021)
26. Wise, B.L., Niu, J., Zhang, Y., Liu, F., Pang, J., Lynch, J.A., Lane, N.E.: Patterns of change over time in knee bone shape are associated with sex. Clinical orthopaedics and related research **478**(7), 1491 (2020)
27. Wu, C.T., Yang, Y.H., Chang, Y.Z.: Three-dimensional deep learning to automatically generate cranial implant geometry. Scientific reports **12**(1), 2683 (2022)
28. Xiang, P., Wen, X., Liu, Y.S., Cao, Y.P., Wan, P., Zheng, W., Han, Z.: Snowflake point deconvolution for point cloud completion and generation with skip-transformer. IEEE Transactions on Pattern Analysis and Machine Intelligence **45**(5), 6320–6338 (2022)
29. Xue, W., Cao, C., Liu, J., Duan, Y., Cao, H., Wang, J., Tao, X., Chen, Z., Wu, M., Zhang, J., et al.: Modality alignment contrastive learning for severity assessment of covid-19 from lung ultrasound and clinical information. Medical image analysis **69**, 101975 (2021)
30. Young, E.Y., Gebhart, J., Cooperman, D., Ahn, N.U.: Are the left and right proximal femurs symmetric? Clinical Orthopaedics and Related Research® **471**, 1593–1601 (2013)